On the Correlation of CO and PAH Emissions from the Combustion of Pulverized Coal and Waste Tires

ARTICLE *in* ENVIRONMENTAL SCIENCE AND TECHNOLOGY · OCTOBER 1998

Impact Factor: 5.33 · DOI: 10.1021/es980399f

2 AUTHORS, INCLUDING:

Yiannis Levendis
Northeastern University
113 PUBLICATIONS **1,988** CITATIONS

Environ. Sci. Technol. **1998**, *32,* 3767−3777

On the Correlation of CO and PAH Emissions from the Combustion of Pulverized Coal and Waste Tires

YIANNIS A. LEVENDIS* AND AJAY ATAL
Department of Mechanical, Industrial and Manufacturing Engineering, Northeastern University, Boston, Massachusetts 02115

JOEL B. CARLSON
U.S. Army Natick R,D&E Center, Natick, Massachusetts 01760

Results are presented on the correlation of the emissions of carbon monoxide (CO) and polynuclear aromatic hydrocarbons (PAH) from the combustion of pulverized bituminous coal and tire-derived fuel. The particle size cuts of coal and tire crumb were 63−75 and 180−212 μm, respectively. Combustion experiments were conducted in laboratory-scale facilities under controlled conditions. The relation between CO and PAH species in the combustion effluent was investigated at drop-tube furnace gas temperatures, in the range of 1000−1300 °C, and several fuel mass loadings in the furnace, expressed in terms of bulk equivalence ratios in the range of 0.7−2.4. Up to 60 two−seven ring PAH compounds were detected by capillary gas chromatography−mass spectrometry (GC−MS) techniques. Results showed that both CO and PAH emission yields increased with increasing bulk equivalence ratio (in the aforementioned range) at a fixed gas temperature. The CO and especially the PAH yields from tire-derived fuel were much higher than those from coal, but the relative amounts of individual PAH components were remarkably similar in the combustion effluent of the two fuels. At fixed bulk equivalence ratios, however, as the furnace gas temperature increased the PAH yields from both fuels decreased drastically, while the CO yields increased. At the highest temperature tested herein (1300 °C), the effluent of the combustion of both fuels was practically devoid of PAHs [at a detection limit of 0.7 μg of a PAH component/g of fuel burnt]. Reasons for the observed increase in CO with temperature are discussed. CO_2 and NO_x emission yields were also monitored, and the results are reported herein.

Introduction

This paper reports on the emissions of polynuclear aromatic hydrocarbon (PAH) and carbon monoxide (CO) from the combustion of coal and waste tire-derived fuel (TDF). PAHs constitute a group of organic hazardous air pollutants of foremost importance because of the toxicity, carcinogenicity, and mutagenicity of some of its components (*1*−*3*). Carbon monoxide is also a toxic gas since it has been known to have a high affinity for haemoglobin, and thus, it is able to displace oxygen in the blood. This can lead to cardiovascular and neurobehavioral effects, and at high concentrations to asphyxiation. Both coal and TDF, in pulverized form, were injected and burned in a laboratory-scale, drop-tube furnace at different gas temperatures, T_g, and particle number densities, i.e., bulk (global) equivalence ratios, ϕ. The effects of these two important parameters of combustion (T_g and ϕ) of solid fuels on the emissions of PAHs and CO were monitored at a fixed furnace gas residence time. Since individual PAH measurements are labor- and time-consuming to conduct with current techniques, it is of technological interest to study whether a correlation exists with the readily measurable CO. There is a debate in the literature on whether CO and unburned hydrocarbon emissions, such as PAHs, correlate (*4*). Some studies reported satisfactory correlations, see refs *5* and *6*, while others did not reveal correlations, see refs *7* and *8*. Some studies used large-scale turbulent flames and were geared to situations in industrial furnaces. In experiments where reactors with water-cooled walls, incomplete mixing, or localized cooling were used, emissions of substantial quantities of products of incomplete combustion (PICs) were seen. Staley et al. (*7*) conducted a comprehensive study on highly volatile hydrocarbon emissions (no PAHs were monitored) from the combustion of two chlorinated C_1 and C_2 hydrocarbons and did not observe any clear correlation with CO. Their investigation faced some uncertainties because it was conducted in the fuel-lean region, where ideally there are no significant CO and unburned hydrocarbon emissions. In such a case, emissions probably resulted from fluctuations in mixing and localized quenching of the flame. While that approach was useful in understanding practical incineration, it most likely resulted in the uneasy task of averaging low concentration profiles of emissions with occasional process upsets (spikes in concentration). Convincing arguments were used to suggest that no correlation was expected. Practically, hydrocarbon emissions are products of pyrolysis, and CO is a product of incomplete oxidation. Hence, in a pyrolytic (oxygen-free) environment, PAH emissions may be present (depending on the temperature) but no CO is expected to form. This was clearly demonstrated in this laboratory (*9*−*11*), as more PAH emissions from waste fuels were released under high-temperature pyrolytic conditions (in N_2) than under oxidative conditions. One of the goals of this work is to further examine the conclusions of Staley et al. (*7*) but this time by conducting combustion experiments under well-characterized laminar and isothermal conditions. Emphasis is given to globally fuel-rich environments ($\phi > 1$), where both CO and PAHs are expected to form in large quantities. Experiments were conducted at four different gas temperatures, in the range of 1000−1300 °C.

TABLE 1. Composition of Ground Waste Tire and Bituminous Coal (HVBA, Pittsburgh no. 8)

property	TDF	coal
particle size (μm)	180−212	63−75
fixed carbon (%)	21.7	51.9
volatiles (%)	52.3	34.4
ash (%)	26.0	13.7
carbon (%)	60.9	71.9
hydrogen (%)	5.3	4.7
sulfur (%)	2.46	1.36
nitrogen (%)	0.28	1.36
oxygen (%)	7.1	7.0
heating value (MJ/kg)	29	29.2

* Corresponding author telephone: (617)373-3806; fax: (617)373-2921; e-mail: yal@artemis.coe.neu.edu.

10.1021/es980399f CCC: $15.00
Published on Web 10/17/1998

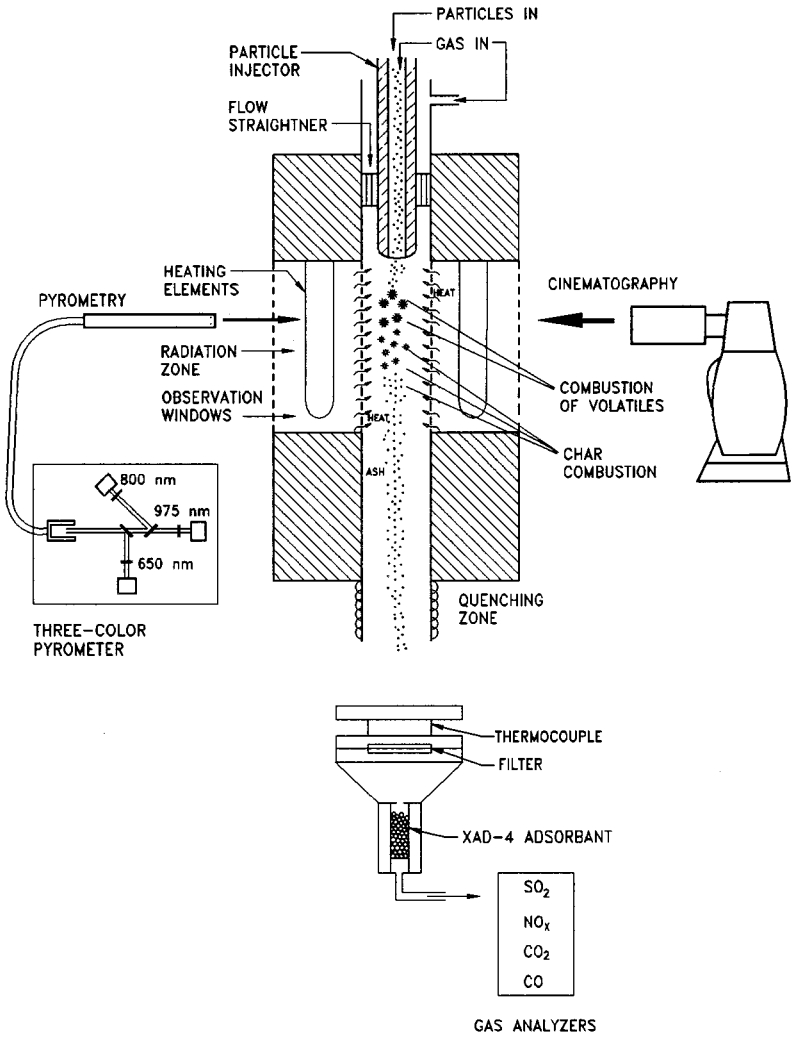

FIGURE 1. General schematic showing features of the drop-tube furnaces used for pyrometric/cinematographic combustion observations and for combustion and emission measurements of dry-injected cylindrical streams (clouds) of particles.

Experimental Section

Fuel Properties. Tire-derived fuel (TDF) was produced by cryogenic grinding of waste tires and was obtained from Midwest Elastomers Inc. The high volatile bituminous coal (Pittsburgh no. 8, HVAB, PSOC-1451) was obtained from the Pittsburgh Coal Bank. The elemental compositions of both the TDF and the coal are given on a moisture-free basis in Table 1, along with other properties. This particular batch of tire crumb had higher ash and sulfur content than what is expected, based on typical values (*6, 12*). The size of pulverized coal was 63−75 μm, which is typically burned in utility boilers. The size of tire crumb was selected to be 180−212 μm, since such particles were found to experience similar total burn times as those of the aforementioned smaller coal particles, see ref *13*.

Combustion Apparatus and Procedure. A laminar-flow, electrically heated, drop-tube furnace (4.8 kW max) was used in this study. The details of the furnace are provided elsewhere (*9, 13, 14*). A simplified schematic showing key features of the vertical furnace is depicted in Figure 1. To introduce fuel to the furnace, a bed of particles was placed in a vibrated glass vial, which was advanced by a constant velocity syringe pump (Harvard Apparatus). Fuel particles from the top of the bed were entrained in a regulated stream of air and were introduced to the furnace through a water-cooled injector (*15, 16*). The furnace has an isothermal radiation zone, 25 cm long and 3.5 cm in diameter. The effluent from the combustion of the resulting cylindrical streams of particles in the furnace (aerosols) was monitored. Gas was introduced into the furnace through the furnace injector and also through a concentric flow straightener, where it was preheated to about 80% of the radiation cavity temperature. Furnace wall temperatures (T_w) were continuously monitored by type-S thermocouples embedded in the wall. Gas temperatures (T_g) inside the furnace were measured at various axial and radial positions by an aspirated shielded thermocouple (suction pyrometer), see refs *16* and *17*. The gas temperature profile along the centerline of the furnace was found to be fairly isothermal in the radiation zone (see ref *14*, Figure 2 and ref *16*); $T_w - T_g \approx 50$ °C.

Furnace gas temperatures were varied from 1000 to 1300 °C. The injection rate of the powders was in the range of 0.3−1.1 g/min, and the total mass flow rate of air varied from 3.9 to 5.1 g/min. This resulted in calculated overall bulk (global) equivalence ratios, ϕ, which varied between 0.7 and 2.4 for both fuels. [Please note that the bulk (global) equivalence ratio was defined as $\phi = m_{fuel}/m_{air})_{actual}/(m_{fuel}/m_{air})_{stoichiometry}$. The bulk equivalence ratio is equal to the inverse of the excess air ratio, λ, which is also called stoichiometric ratio.] Thus, a range of combustion conditions from fuel-lean to fuel-rich were examined. This range addresses most practical combustion applications. Each experiment lasted between 2 and 4 min. Gas flow rates through the furnace (at STP) were adjusted for the different

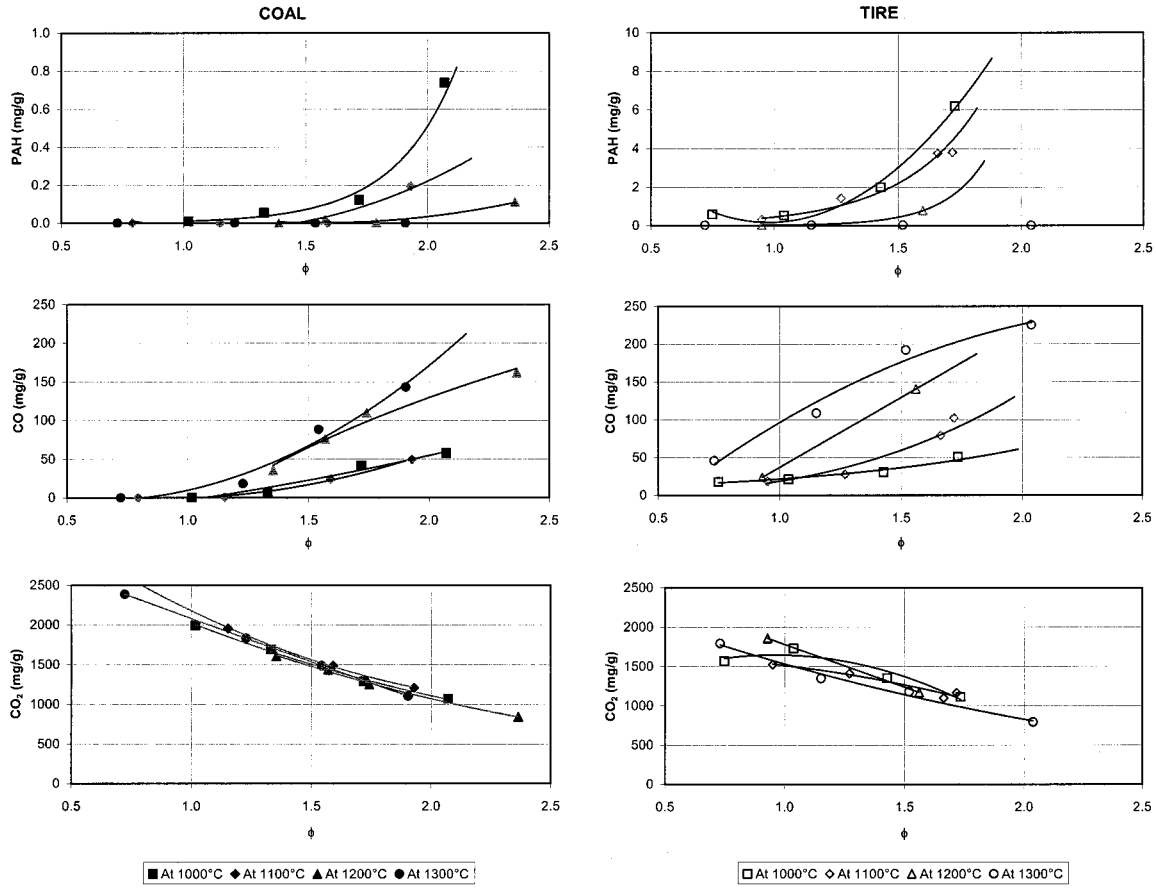

FIGURE 2. Emission yields (mg/g of fuel fed to the furnace) of (a) first row PAHs, (b) second row CO, and (c) third row CO_2. All emissions are plotted against the bulk equivalence ratio, ϕ, for four furnace gas temperatures: 1000 (□), 1100 (◊), 1200 (△), and 1300 °C (○). Left column corresponds to emissions from coal (solid symbols); right column corresponds to emissions from tire (open symbols).

gas temperatures, resulting in a gas residence time in the isothermal zone of ≈0.75 s. Pyrometry and cinematography of burning single particles and cylindrical streams of particles were performed in a separate furnace of similar architecture, and the results were described in refs *13* and *18*, respectively.

Combustion Emissions Monitoring. At the exit of the isothermal cavity of the furnace, the effluent gases were cooled at a rate a little under 10^3 °C/s (*16*). Cumulative emissions of all the PAH species were monitored by passing the entire flow of the furnace through a sampling stage (Graseby), containing a filter and a glass cartridge with XAD-4 adsorber. The effluent gases were subsequently passed through a Permapure dryer to remove moisture. Thereafter, they were channeled to continuous flow analyzers to measure emissions of CO and CO_2 (Horiba infrared) and NO_x (Beckman 951A chemiluminescent NO/NO_x). The output of these analyzers was recorded using an Omega analog-to-digital converter in a microcomputer. The signals from the analyzers were recorded for the duration of the fuel powder injection, and subsequently, they were converted to partial pressures.

Sampling, Extraction, and Analysis of PAHs The EPA Method TO-13 for sampling PAHs in ambient air was used for the sampling, extraction, and analysis of PAH components in furnace effluents. Modifications were employed to allow adaptation of this method to the apparatus shown in Figure 1. The lower range of detection for the GC−MS was 0.7 μg/g as the GC−MS system was operated in the full-scan mode to enhance PAH identification, and a split ratio of 2.7:1 was used to accommodate the large range in sample concentrations. [To verify the GC−MS modifications, a comparison of the GC−MS method employed herein and the GC−MS method in EPA Method TO-13 was conducted with NIST Standard Reference Material 1597. The results indicated insignificant differences between the qualitative or quantitative aspects of SRM 1597.]

The sampling stage for PAHs was located directly below the furnace, Figure 1, enabling the entire furnace effluent to pass through. Particulate emissions containing condensed phase PAHs were captured on a 0.45-μm pore size glass fiber filter, while the gaseous-phase PAHs were adsorbed onto a bed of XAD-4 resin located beneath the filter. The temperatures of the filter and the XAD-4 resin were measured at ≈90 and 70 °C, respectively. Given that the PAH distribution in the particulate and vapor phases is sensitive to the filter stage temperature but their sum is not (*19, 20*), it was decided to present results herein as combined gaseous and condensed phase PAHs. [The dew point temperature of the exhaust gases was under 60 °C in all experiments, thus no water condensation was expected in the sampling stages.] Under the conditions of this sampling, more PAHs were detected in the condensed phase.

Following combustion, the glass fiber filter and XAD-4 resin were spiked with 100 μg of naphthalene-d_8 and extracted with methylene chloride in a precleaned Soxhlet apparatus (*9, 18*). After extraction, the methylene chloride solutions were concentrated to 1 mL under low vacuum. Details are given in ref *9*.

The concentrated samples were spiked with an 100 μg aliquot of anthracene-d_{10}. A comparison of the peak areas for the naphthalene-d_8 and anthracene-d_{10} in the total ion chromatogram (TIC) provided a measure for the extraction/condensation efficiency and was used as a basis for the data provided herein. Identification was limited primarily to species found in Title III of the 1990 Clean Air Act Amend-

ments. The GC−MS system consisted of a Hewlett-Packard (HP) Model 5809 GC equipped with a HP Model 5971 mass selective detector. The GC−MS conditions and data reduction techniques were described previously (*9, 11*). No PAHs were detected in laboratory blanks (plain XAD-4 extracts) or combustion blanks (sampling the furnace exhaust at the absence of fuel).

To assess the reproducibility of the PAH analysis, several experiments were repeated, and a standard deviation of 10% was observed. The source of this experimental error resulted from a combination of the sampling, concentration, and analysis techniques. The experimental procedure was kept consistent in all tests in order to ensure the validity of relative trends. Limited statistical data on reproducibility has been described previously (*9*).

Results and Discussion

Emissions of PAHs, CO, and CO_2 from Coal and TDF. In several of the fuel-rich combustion experiments up to 60 different PAH species were identified and quantified. The PAH compounds ranged in size from two fused-ring structures, like naphthalene (MW = 128), up to seven fused-ring structures, such as coronene (MW = 300). [Please note that the GC−MS detection efficiency for the large multi-ring PAHs is expected to be low because of the low volatility of these compounds.] The yields of all PAHs of both fuels, at the exit of the furnace, are listed in Tables 2 and 3 for coal and tire crumb, respectively. The cumulative emission yields of the sums of all PAH components are listed at the bottom of Tables 2 and 3 and are also plotted in Figure 2, first column, as a function of the bulk equivalence ratio ϕ and temperature.

Trends of several selected individual PAH yields with bulk ϕ are shown in Figure 3. Anthracene, phenanthrene, pyrene, fluoranthene, acephenanthrylene, benzo[*ghi*]fluoranthene, cyclobenzo[*cd*]pyrene and benzo[*a*]pyrene were selected for presentation because they were either predominant or because some have been repeatedly reported to be highly toxic. The PAH emissions shown in Tables 2 and 3 as well as in Figures 2 and 3 represent the sum contribution from both gaseous and condensed phases. While in this study most of the PAHs were found to be in the condensed phase, this was probably due to the low temperature of the filter stage, as mentioned earlier. The highest amounts of PAHs were most noticeably observed under low temperatures−high ϕ conditions, in the ranges examined herein. The lowest amounts of PAHs were observed under fuel-lean conditions or at high combustion temperatures.

The evaluation of the cumulative PAH emissions for coal and TDF, shown in the first column of Figure 2 and in Figure 3, make evident the following trends: The PAH emissions increased exponentially in the fuel-rich domain, and an increase in combustion temperature resulted in a dramatic reduction in cumulative PAH yields. The PAHs could have been oxidized (fully or, most likely, partially) or could have resulted in larger condensed structures, i.e., soot. The cumulative PAH emissions from combustion of TDF were a full order of magnitude larger than those from coal (note the different scales chosen for display on the ordinate axis of Figure 2). The exponential decrease in PAH emissions from TDF occurs at a much lower ϕ than observed for coal. At the highest temperature of this study, T_{gas} = 1300 °C, no PAHs were found at the detection limit of 0.7 μg/g of this technique. As expected, similar trends were observed when individual PAH species were examined (Figure 3). The trends of the individual PAH emission components from the two fuels were remarkably similar under similar combustion conditions. The following explanations are offered for this observed phenomena: Tire-derived fuel contains a larger amount of volatiles than coal (see Table 1), and the release of these volatiles readily creates diffusion-controlled common flames. Such flames engulf groups of particles as the particle number density, and thus, bulk ϕ increases in the furnace. Pulverized coal contains much less volatile matter (see Table 1), and its combustion resists the formation of common flames until higher equivalence ratios (than those for the TDF fuel) are reached. This was demonstrated with high-speed cinematographic studies in ref *18*, highlights of which are also illustrated herein in Figure 4.

There are several trends that both CO and PAH emissions have in common. First, both PAH yields and CO yields from the two fuels increase sharply with ϕ in the fuel-rich domain, at the lower gas temperatures. Second, the sharp increase in both PAH and CO yields occurs at a lower bulk ϕ for tire-derived fuel than for coal. For both fuels, the CO partial pressure increased from very low levels at $\phi < 1$ to a maximum of 5.5% atm at $\phi = 2$. The latter figure accounted for as much as 16% of the fuel carbon content. However, the trend exhibited by the CO emissions, with furnace gas temperature, was opposite to the trend exhibited by the PAH emissions. The CO emissions increased with increasing gas temperature. This trend was clearly observed for both fuels, as illustrated in Figures 2, second row, and 5, first row. The relative increase in CO emissions was as much as a factor of 3, as the gas temperature rose by 300 °C (from 1000 to 1300 °C). Possible explanations are offered in the ensuing section.

CO_2 yields from burning TDF were lower (5−10%) than those from coal, which reflects its lower carbon content. CO_2 yields from both fuels experienced a declining trend with the equivalence ratio, particularly in the fuel-rich domain. As the combustion efficiency decreased with ϕ in this range, increasing amounts of carbon (char) remained unburned. Moreover, the emissions of CO increased with ϕ, as mentioned above. Thus, the major pathways that explain the decline of the CO_2 yields are the increasing CO and carbon (char, tars, soot) yields. There was no clear trend in the CO_2 yields with the gas temperature.

The NO_x emissions from the two fuels were extensively studied in separate investigations (*9, 21*). Nevertheless, testing was also conducted herein, and the results are summarized in the following. NO_x emissions of tire crumb were much lower, by a factor of 3−4, than those of coal. This reflected the much lower fuel-nitrogen content of tires (see Table 1). NO_x emissions of both fuels decreased drastically, by a factor of 5, with increasing bulk ϕ in the range examined herein because of lower flame temperatures and local oxygen partial pressures (*18*). NO_x emissions increased mildly with increasing gas temperature.

Discussion on the Individual PAH Component Yields. The individual PAH components (combined gas and condensed phase, as explained in a prior section) are listed in Tables 2 and 3, under all the conditions of these experiments. At the lowest temperature of this study (1000 °C), a large number of PAH species were recorded in the effluent of tire crumb combustion, the sum of which increased with the equivalence ratio, and reached 50 at the most fuel-rich conditions examined ($\phi = 1.7$). Clearly, both the number of components and their respective quantities were reduced as the furnace temperature was progressively increased to 1300 °C. At this highest temperature no PAHs were detected with the exception of acenaphthylene, which was present in small amounts. The trends of the PAH emissions from coal with ϕ and T_{gas} were similar to those from TDF, but both the number of detected species and the associated quantities were much lower. At 1300 °C, no PAHs were present in coal combustion effluents at the detection limit of this study, 0.7 μg/g of fuel.

By examining the combustion conditions of this study that emitted the largest number and quantities of PAHs for both fuels, i.e., a temperature of 1000 °C and strongly fuel-

TABLE 2. PAH Yields from the Combustion of Pulverized Coal[a]

T_{gas} (°C)	1000				1100				1200				1300			
mass burned (g)	2.21	1.80	2.32	2.23	0.79	1.16	0.80	1.13	1.57	1.10	1.62	2.20	1.06	1.26	1.28	0.99
equivalence ratio (ϕ)	1.02	1.33	1.72	2.07	0.79	1.15	1.59	1.93	1.39	1.58	1.79	2.36	0.73	1.21	1.54	1.91
indene (116)				20												
naphthalene (128)	8	34	66	192				89		18		52				
benzothiophene (134)				11								3				
2-methylnaphthalene (142)				12												
methylthiophene (148)																
1-methylnaphthalene (142)				9												
biphenylene (152)				3												
biphenyl (154)	1			6												
acenaphthylene (152)		12	39	141				53				42				
acenaphthene (154)				2												
naphthalene carbonitrile (153)				9												
dienzofuran (168)				8												
fluorene (166)				18												
2-methylfluorene (180)																
9*H*-fluoren-2-one (180)				2												
dibenzothiophene (184)				8												
phenanthrene (178)		7	10	66				11				3				
anthracene (178)				14												
carbazole (167)																
methyl dibenzothiophene (198)																
ethenyl anthracene (204)				4												
3-methylphenanthrene (192)				2												
2-methylphenanthrene (192)				2												
2-methylanthracene (192)																
4*H*-cyclopenta[*def*]phenanthrene (190)				11								2				
fluoranthene (202)		2	4	46				14				2				
acephenanthrylene (202)				16												
phenanthro[4,5-*bcd*]thiophene (208)				16								2				
pyrene (202)			4	42				22				4				
benzo[*b*]naphtho[2,3-*d*]furan (218)				2												
benzo[*a*]fluorene (216)				4												
benzo[*b*]fluorene (216)				4												
1-methylpyrene (216)				1												
benzo[*b*]naphtho[2,1-*d*]thiophene (234)				1												
benzo[*ghi*]fluoranthene (226)				7												
benzo[*c*]phenanthrene (228)				3												
benzo[*b*]naphtho[1,2-*d*]thiophene (234)																
benzo[*b*]naphthio[2,3-*d*]thiophene (234)																
4*H*-cyclopenta[*cd*]pyrene (226)				17				5								
benzo[*a*]anthracene (228)				6												
chrysene triphenylene (228)				4												
benzo[*b*]fluoranthene (252)				4												
benzo[*j*]fluoranthene (252)																
benzo[*k*]fluoranthene (252)				5												
benzo[*a*]fluoranthene (252)				3												
benzo[*e*]pyrene (252)				3												
benzo[*a*]pyrene (252)				5												
perylene (252)				1												
indeno[7,1,2,3-*cdef*]chrysene (276)																
dibenz[*a,j*]anthracene (278)																
indeno[1,2,3-*cd*]pyrene (276)				1												
dibenzo[*a,h*]anthracene (278)																
benzo[*b*]chrysene (278)				3												
picene (278)				2												
benzo[*ghi*]perylene (276)				3												
anthanthrene (276)																
naphtho[1,2-*k*]fluoranthene (302)																
dibenzo[*b,k*]fluoranthene (302)																
coronene (300)																
dibenzopyrene (302)																
total (in mg/g (exec. naphthalene)	0.001	0.021	0.057	0.527				0.106				0.058				
total (in mg/g)	0.009	0.055	0.123	0.739				0.195		0.018		0.110				

[a] Individial PAH yields in μg/g. Total PAH yields in mg/g.

rich conditions ($\phi \approx 2$), several observations may be made. Within the same sample: (a) The yields of naphthalene and acenaphthylene were higher than the rest of the species. The amounts of these two species were comparable, with those of acenaphthylene being generally less (in agreement with results reported by Longwell for premixed flames; *2*), except at the higher gas temperatures (1200 and 1300 °C) for tire crumb. At those conditions, acenaphthylene appeared to be the most predominant species and proved difficult to eliminate completely. (b) Phenanthrene, fluoranthene, and pyrene were the next most prominent compounds. The yields of phenanthrene were higher than those of pyrene and fluoranthene at the lower temperatures. This was reversed at the higher temperatures, indicative of a higher activation energy for phenanthrene. The yields of the isomer species pyrene and fluoranthene ($C_{16}H_{10}$) were strikingly

TABLE 3. PAH Yields from the Combustion of Tire Crumb[a]

T_{gas} (°C)	1000				1100				1200		1300			
mass burned (g)	1.32	1.22	1.26	1.67	1.04	1.39	1.06	1.10	1.17	1.44	1.14	1.17	1.20	1.38
equivalence ratio (ϕ)	0.75	1.04	1.43	1.73	0.95	1.27	1.66	1.72	0.95	1.6	0.72	1.15	1.52	2.04
indene (116)				47										
naphthalene (128)	198	206	542	1368	138	165	504	564	17	134			8	
benzothiophene (134)	20	28	76	139		44	89	94		18				
2-methylnaphthalene (142)			6	23		10								
methylthiophene (148)														
1-methylnaphthalene (142)			3	16		8								
biphenylene (152)	3	2	10	35										
biphenyl (154)	15	13	38	104	7	35	43	49		9				
acenaphthylene (152)	88	107	365	937	67	328	619	665		235	15	25	13	8
acenaphthene (154)	3		4	22										
naphthalene carbonitrile (153)			4	20										
dienzofuran (168)			2	9										
fluorene (166)	6	7	27	102		21	29	35		6				
2-methylfluorene (180)				10										
9*H*-fluoren-2-one (180)			3	6										
dibenzothiophene (184)	9	8	33	103	4	25	56	66		9				
phenanthrene (178)	71	63	281	1035	27	85	174	197		23				
anthracene (178)	10	9	39	156		11	20	23						
carbazole (167)														
methyl dibenzothiophene (198)														
ethenyl anthracene (204)	6	2	21	92										
3-methylphenanthrene (192)				10										
2-methylphenanthrene (192)				10										
2-methylanthracene (192)														
4*H*-cyclopenta[*def*]phenanthrene (190)	5	4	20	66		19	48	41		9				
fluoranthene (202)	38	28	145	482	24	139	381	376		57				
acephenanthrylene (202)	12	9	49	169	5	40	98	103		13				
phenanthro[4,5-*bcd*]thiophene (208)	4	4	17	47	4	24	65	61		19				
pyrene (202)	32	25	125	421	27	143	414	406		107				
benzo[*b*]naphtho[2,3-*d*]furan (218)														
benzo[*a*]fluorene (216)				20										
benzo[*b*]fluorene (216)			5	15										
1-methylpyrene (216)														
benzo[*b*]naphtho[2,1-*d*]thiophene (234)	1		5	22			13	20						
benzo[*ghi*]fluoranthene (226)	8	4	24	71	6	38	83	94		18				
benzo[*c*]phenanthrene (228)	1		5	20			19							
benzo[*b*]naphtho[1,2-*d*]thiophene (234)				4										
benzo[*b*]naphthio[2,3-*d*]thiophene (234)				9										
4*H*-cyclopenta[*cd*]pyrene (226)	10	5	39	128	6	80	277	261		54				
benzo[*a*]anthracene (228)	5		12	48		16	33	34						
chrysene/triphenylene (228)	7		15	60		7	31	46		18				
benzo[*b*]fluoranthene (252)			8			40	123	114						
benzo[*j*]fluoranthene (252)														
benzo[*k*]fluoranthene (252)	11		18	102										
benzo[*a*]fluoranthene (252)	2		6	24		11	25	36						
benzo[*e*]pyrene (252)	4		9	30		19	42	56		10				
benzo[*a*]pyrene (252)	6		13	65		28	110	99		13				
perylene (252)			2	10		7	22	21						
indeno[7,1,2,3-*cdef*]chrysene (276)				9		20	32	29						
dibenz[*a,j*]anthracene (278)				19										
indeno[1,2,3-*cd*]pyrene (276)	3		8	39		21	102	88		11				
dibenzo[*a,h*]anthracene (278)				9										
benzo[*b*]chrysene (278)														
picene (278)														
benzo[*ghi*]perylene (276)	7		7	36		31	164	113		12				
anthanthrene (276)				22		10	65	54						
naphtho[1,2-*k*]fluoranthene (302)				10										
dibenzo[*b,k*]fluoranthene (302)														
coronene (300)							74	67						
dibenzopyrene (302)				5										
total (in mg/g (exec. naphthalene)	0.386	0.316	1.447	4,789	0.178	1.258	3.250	3.245		0.640	0.015	0.025	0.013	0.008
total (in mg/g)	0.584	0.523	1.989	6.204	0.315	1.424	3.754	3.809	0.017	0.774	0.015	0.025	0.021	0.008

[a] Individial PAH yields in μg/g. Total PAH yields in mg/g.

analogous (which has also been reported by Longwell (*2*) for toluene and acetylene flat flames as well as for combustion in diesel engines and gasoline engines). However, pyrene proved to be more resistant to increasing temperature than fluoranthene. (c) Cylopenta[*cd*]pyrene was the next sizable component, with yields lower than those of pyrene by factors of 2−3 at 1000 and 1100 °C and by a factor of 4 at 1200 °C. (d) The yield of benzo[*a*]pyrene was lower than that of cyclopenta[*cd*]pyrene by an additional factor of 5. The isomer species benzo[*a*]fluoranthene and benzo[*a*]pyrene ($C_{20}H_{12}$) were also present in large amounts at their most favorable conditions (low T_g − high ϕ), the latter species being obtained in larger yields. Given the completely different nature and origins of coal and tire crumb fuels, the similarities of the relative amounts of PAH yields from their combustion and the observed similar trends with ϕ and T_g are notable. Such

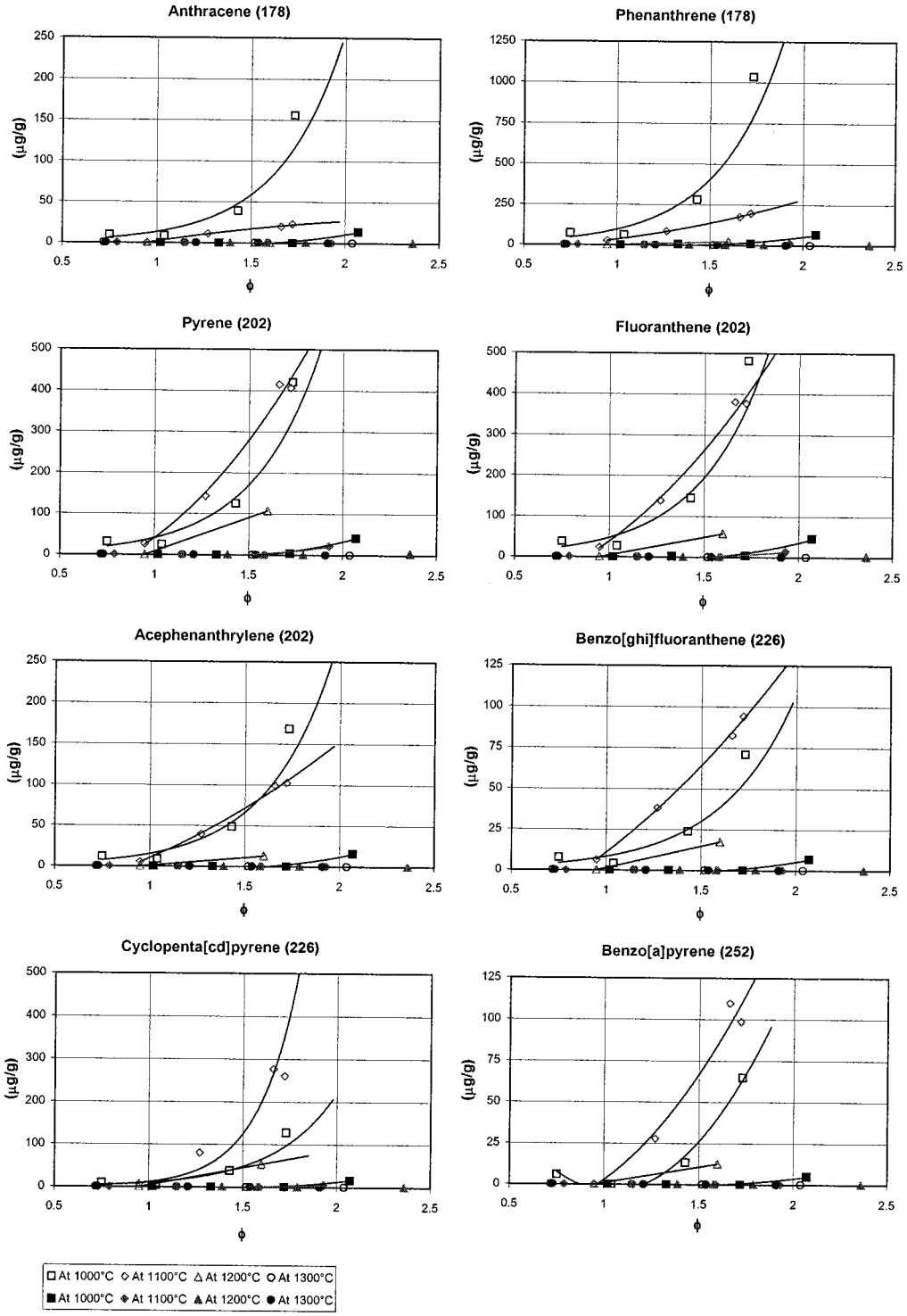

FIGURE 3. Emission yields (μg/g of fuel fed to the furnace) of selected PAH compounds: anthracene, phenanthrene, pyrene, fluoranthene, acephenanthrylene, benzo[*ghi*]fluoranthene, cyclopenta[*cd*]pyrene, and benzo[*a*]pyrene. All emissions are plotted against the bulk equivalence ratio, ϕ, for four furnace gas temperatures: 1000 (□), 1100 (◇), 1200 (△), and 1300 °C (○). In each plot, the emissions of coal and tire are superimposed. Tire emissions: open symbols; coal emissions: solid symbols.

similarities indicate that the formation and, of course, the oxidation of PAHs occurs by similar mechanisms.

Discussion on the CO Yields. An investigation was conducted to determine why the CO emissions increased with the gas temperature. Such a trend became especially obvious when coal and tire were burned in the fuel-rich domain. As the local equivalence ratios are not known, it is not easy to find an explanation to account for such a rather large increase in CO yields (by a factor of 3−4) with increasing gas temperature, in the 1000−1300 °C range. Certainly contributions to the increase in CO emissions with temperature can be attributed to the partial oxidation of hydrocarbons (aliphatics and aromatics) as was strongly indicated by the reductions in PAHs. Contributions are also due to enhanced oxidation of char, since the yield of unburned char mildly decreased with increasing gas temperature. However, such measured contributions were not sufficient to explain the magnitude of the observed increase

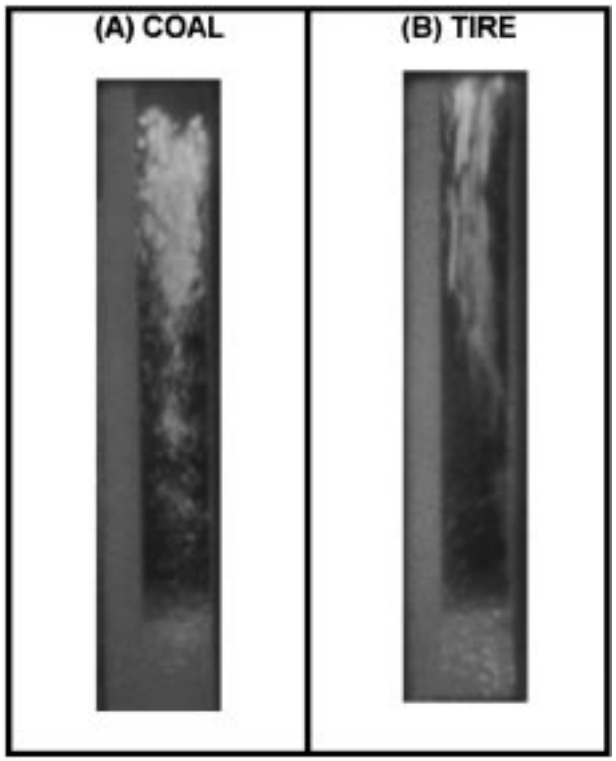

FIGURE 4. Snapshots of high-speed photography of burning cylindrical streams of particles of coal (63−75 μm) and tire particles (180−212 μm) at an approximate ϕ of 1.4. High-speed photographs were taken with a Hycam II camera. Pyrometry was performed with a near-infrared three-color pyrometer. Recorded temperatures were (a) 1500 ° C for the volatile flame combustion for coal and (b) 1400 °C for the volatile flame combustion for tires. Combustion occurred in air at T_{gas} = 1100 °C. Char combustion temperatures were ≈100 °C above the gas temperature. Complete photographic studies can be found in refs *13* and *18*.

in CO yields. To investigate this situation further, equilibrium calculations were performed using the STANJAN equilibrium code (*22*) at the aforementioned temperatures and atmospheric pressure. Beside the stated parameters, input to this code were the relative atomic populations of C, O, H, and N at the conditions of the experiments ($0.5 < \phi < 2$). Twenty species were selected as representative of the situation, including CO, CO_2, H_2O, H, H_2, OH, N, NO, NO_2, and several hydrocarbons, such as CH_4, C_3H_8, C_2H_2, C_6H_6, etc., which in a non all-inclusive manner could represent volatiles. The program then solves for the equilibrium state using the method of element potentials. With these assumptions, the calculated equilibrium CO and CO_2 concentrations in the coal combustion effluent are plotted with global ϕ and T_g in the second row of Figure 5. The measured concentrations are plotted in the top row. The overall trends of the experimental data and of the calculated equilibrium values with changing ϕ bear resemblances. The CO emissions start from very low values in the fuel-lean domain and then drastically rise in the fuel-rich domain. The CO_2 emissions rise slowly to a maximum around stoichiometry and then fall slowly, again, in the fuel-rich domain. The magnitudes of the concentrations are comparable in the fuel-lean domain and at stoichiometry, but they are not in agreement in the fuel-rich domain, where the equilibrium model overpredicts the CO and underpredicts the CO_2 (by a factor of ≈6 at ϕ = 2). Furthermore, the model predicts the experimentally observed trend of increasing CO concentrations with increasing furnace temperature; however, the magnitude of the increase is far less than that observed experimentally in the fuel-rich domain. For instance, as T_g is raised from 1000 to 1300 °C, the CO emissions are predicted to increase by under 10% in the examined fuel-rich domain. This is much less than the factor of 3−4 observed experimentally. Thus, the system does not appear to be in chemical equilibrium.

An explanation for the observed magnitude of the increase of CO emissions with gas temperature may be based on the increasing amounts of CO released as a primary product of solid carbon oxidation. Solid carbon is found in the forms of soot and unburned char in the fuel-rich domain. Indeed, several studies have documented the increase of primary product CO/CO_2 ratio from combustion of carbon with

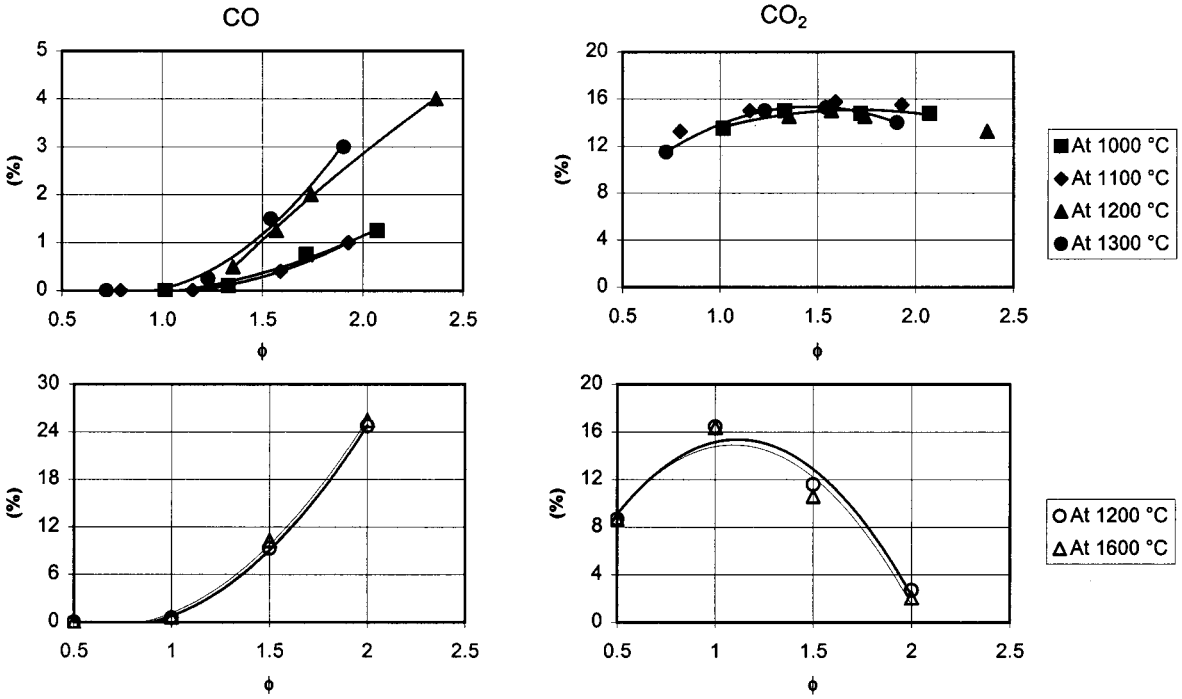

FIGURE 5. Top row: Actual emissions (% atm) of CO and CO_2 from combustion of pulverized coal (corresponding to the yields shown in Figure 2) at various gas temperatures and global equivalence ratios in the furnace. Bottom row: Calculated emissions (% atm) of CO and CO_2 using an equilibrium scheme (Stanjan).

TABLE 4. Co/Co_2 Ratio as Primary Product of Carbon Oxidation

investigator	material/system	expressions for CO/CO_2	range of validity T_p (K)	range of validity P_{O_2} (atm)
Tognotti et al. (*27*)	spherocarb/EDB	$50\ P_{O_2}^{-0.21} \exp\left(\frac{-3000}{T_p}\right)$	670−1670	0.05−1.0
Zeng and Fu (*31*)	carbon/thermobalance	$600\ (\rho_s Y_{O_{2,s}})^{-0.24} \exp\left(\frac{-8000}{T_p}\right)$	900−1600	0.4−4.0
Arthur (*23*)	graphite/flow system + $POCl_3$	$10^{3.4} \exp\left(\frac{-12400}{RT_p}\right)$	730−1170	0.24−0.5
Rossberg (*24*)	electrode carbons/flow systems	$10^{3.3} \exp\left(\frac{-14300}{RT_p}\right)$ or $10^{3.9} \exp\left(\frac{-18700}{RT_p}\right)$	790−1690	
Hurt and Mitchell (*30*)	PSOC-1451 char/laminar-flow reactor	$4 \times 10^4 \exp\left(\frac{-30000}{RT_p}\right)$	1500−2000	0.06−0.12

[a] Note: R is 1.987 cal/mol.K, and ρ_s is density of air at surface of particle in kg/m^3.

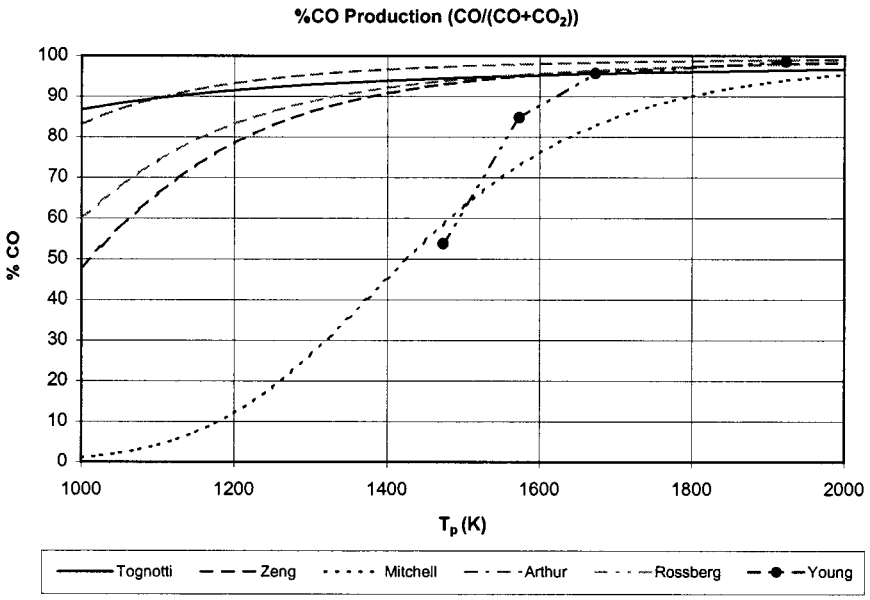

FIGURE 6. CO/CO_2 ratio as primary products of the oxidation of carbonaceous materials and coal chars. Various semiempirical relationships, listed in Table 2, are plotted against carbon surface temperature. Whenever applicable, the oxygen partial pressure in the bulk was assumed to be 0.005 atm; the surface oxygen partial pressure was assumed to be half of the bulk.

temperature in the aforementioned temperature range at various oxygen partial pressures. Such studies include the work of Arthur (*23*), Rosseberg (*24*), Phillips et al. (*25*), Young and Niksa (*26*), Tognotti et al. (*27*), Mitchell and co-workers (*28*−*30*), and Zeng and Fu (*31*) among others. These investigators examined the high-temperature oxidation of various forms of carbon, using different direct or indirect measurements, and provided empirical correlations of the primary CO/CO_2 product ratio shown in Table 4, where the oxygen partial pressure during those experiments is also tabulated. All correlations show that, as the carbon particle temperatures increase, the formation of CO is more favored over that of CO_2, as illustrated in Figure 6 for char particle temperatures relevant to this study. For this plot, the average oxygen partial pressure, P_{O_2}, in the furnace under fuel-rich conditions was assumed to be 0.005 atm (0.5%) based on actual measurements taken at $\phi = 1.5$. This P_{O_2} is lower than those investigated in the aforementioned studies, i.e., $1 > P_{O_2} > 0.05$ atm. The reason for extrapolating the literature data to our lower oxygen concentrations was based on the work of Tognotti et al. (*27*). Therein it was reported that the CO/CO_2 primary product ratio increased with decreasing oxygen partial pressures. Indeed, the largest CO/CO_2 ratio was recorded at the lowest P_{O_2} (0.05 atm) implemented in that study, while the smallest CO/CO_2 ratio was recorded at the highest P_{O_2} (1 atm). For high-purity carbons, such as graphite, soot, synthetic chars, etc. (*23*, *24*, *27*, *31*), it appears that CO is expected to be the dominant product of oxidation in the range of particle temperatures of 1000−2000 K (Figure 6). Correlations for coal char combustion (*26*, *28*−*30*) show larger variability in the products, with CO_2 being the major product below 1000 K and CO being the major product at 2000 K. The fact that coal chars produce much more CO_2 at the lower temperatures than the high-purity carbons (see Figure 6), may be attributed to the effects of catalytic inorganic impurities in the former. Such catalysts are known to promote the formation of CO_2 at lower temperatures, see the discussion by Young and Niksa (*26*). Based on a correlation provided by Hurt and Mitchell (*30*) for the same coal char that was used in this work (PSOC-1451), plotted in Figure 6, it is shown that for a particle temperature [Pyrometric results obtained in this laboratory showed that, under fuel-rich conditions, char particle temperatures were in the order of 100 °C higher than corresponding surrounding gas temper-

atures.] increase from 1100 (1373 K) to 1400 °C (1673 K) the primary CO product doubles at the expense of CO_2. A similar relative change was observed in this work. For instance, at a bulk ϕ of 1.6, the partial pressure of coal-generated CO increased from 0.5 to 1.4% atm as the temperature increased in the aforementioned range, while CO_2 decreased mildly (in the vicinity of 15% atm). Even at $\phi > 1$ there was some oxygen in the bulk gas (<1% atm) because of limited mixing in the laminar flow furnace. Hence, some CO most likely oxidized to CO_2, and absolute concentrations of CO at the exit of the furnace were lower than those released as primary products of char combustion based on Figure 6.

The volatile combustion stage may not be a major contributor to the measured CO levels at the exit of the furnace since the volatiles of the fuels burn in the upper part of the furnace at a distance from the exit (see Figures 1 and 4). Hence, sufficient time should be available for the oxidation of the CO emissions originating therefrom, in the post flame region where char combustion takes place. This is indicated by a simple one reaction calculation (shown below) as well as by the results of separate experiments. In those experiments chars of coal generated at 1200 °C in N_2 were burned in air at conditions similar to the combustion of parent coal at $\phi = 2$. Again, more CO was produced at 1300 than at 1100 ° C (0.5 vs 0.1% atm) at the absence of volatile combustion. In this experiment, soot was absent in the combustion effluent. These lower levels of CO indicate that soot rather than char may be the form of carbon that is responsible for most of the CO emissions during the parent coal combustion, or the combustion of TDF.

The next step of this analysis should investigate whether any enhanced amounts of CO that form at higher gas temperatures, presumably as a primary product of carbon oxidation, have sufficient time in the furnace to oxidize to CO_2. To address this question consider a possible chemical reaction:

$$CO + OH \rightleftharpoons CO_2 + H \qquad (1)$$

Assuming a forward reaction rate constant of

$$k_{+1} = 4.4T^{1.5}e^{372/T} \qquad (m^3\ mol^{-1}\ s^{-1}) \qquad (2)$$

and

$$R_{+1} = k_{+1}[CO][OH] \qquad (3)$$

The characteristic reaction time for oxidation in post-flame regions, as the gases cool, can be defined as (*32*)

$$\tau = [CO]/R_{+1} = 1/(k_{+1}[OH]) \qquad (4)$$

Assuming, as a first approximation, the OH radicals to be present at their equilibrium concentration (see ref *32*) [According to the reaction: $1/2H_2O + 1/4O_2 \rightleftharpoons OH$, where the equilibrium constant $K_{p_{OH}} = 166e^{19\ 680/T}$ (*32*).], the characteristic times for reaction in the isothermal cavity may be calculated. For coal particles burning at a bulk ϕ of 1.6, $T_g = 1000$ °C and P_{O_2} of 0.01 or 0.005, the characteristic time τ is 127 or 126 ms, respectively. But when the gas temperature is raised to 1300 °C, the corresponding characteristic times are calculated to be 8.1 and 8 ms, respectively. [If superequilibrium concentrations of [OH] are assumed, then the calculated characteristic times will be shorter. It was assumed in these calculations that $n_{H_2} = 1/2n_{CO}$; the assumption that $n_{H_2} = 1/4n_{CO}$ results in even shorter characteristic times.] Thus, it is evident that at the lower temperatures of this study insufficient post-flame residence times in the furnace may impede the CO to CO_2 conversion; but the higher temperature residence times are much longer than 8 ms and should result in additional CO_2 conversion, had sufficient oxygen been present. Therefore, to explain the observed trends in CO emissions, attention was directed to the post-flame (char + soot combustion) zone and the cool-down zone. On the basis of the analysis of Fenimore and Moore (*33*), Seinfeld and Flagan (*32*)] presented expressions for the maximum cooling rate beyond which oxidation reactions are expected to be frozen. Using those results (see ref *32*, Figure 3.14) at the cooling rate measured at the exit of this furnace, 10^3 K/s, the CO chemistry is expected to be 'frozen' at or below ≈875 °C, while deviations from partial equilibrium are expected to occur below ≈1125 °C. In the present experiments, the char combustion phase is prolonged at high ϕ, and not all particles extinguish at the end of the radiation zone (see Figure 4 and ref *18*). Also, at high ϕ values, large amounts of soot are present. Thus, burning char and soot particles enter the cool-down zone. Therein, a fraction of the emitted CO becomes frozen. The higher CO emissions from soot and char at the higher furnace temperatures are thus reflected in correspondingly larger amounts of frozen CO that exit the furnace. It is also possible that at the presence of water vapor, generated from the volatile combustion phase, soot and char convert to CO as illustrated by the following reaction scheme: $C + H_2O \rightleftharpoons CO + H_2$ (as the PAH production is decreased). This scheme could partly account for the high levels of CO yield when coal particles were burned, as contrasted to the low levels of CO yield when pre-devolatilized coal char particles were burned (no H_2O was present in the latter case). There is a counter-argument, however, since water has been found to catalyze the homogeneous oxidation of CO to CO_2 at higher temperatures (*27*).

To gain further understanding, similar experiments were conducted involving the combustion of two additional fuels that do not generate chars, poly(styrene) (PS) and poly(methyl methacrylate) (PMMA). Combustion of these two fuels at a $\phi = 1.6$ produced CO emissions that were higher than those of coal and TDF. The CO emissions of these two polymers also increased with temperature in the same range but by a lesser degree (e.g., from 7.5 to 11% atm for PMMA). [It was earlier confirmed in this laboratory that the PAH emissions of PS and PMMA diminish with increasing furnace temperature (*15*), thus, this analysis was not repeated herein.] While no char was generated, large quantities of soot were collected at the exit of the furnace. Again, the above arguments can be applied to soot alone but, as soot is a purer carbon than char, it produces more CO than char and experiences less relative CO/CO_2 product variation in the 1400−1700 K range, in good agreement with the correlations shown in Figure 6. Finally, results confirming the higher CO emissions at increasing furnace temperatures at fuel-rich conditions were also obtained during batch combustion of fixed beds of all the above fuels (pulverized coal, tire, poly(styrene) and poly(methyl methacrylate) in a horizontal muffle furnace (see Figure 3 of ref *15*) as long as soot was present at the exit of the furnace.

Summary

An experimental study was conducted to assess the correlation (or lack of) between CO and PAH emissions from the combustion of solid fuels. Pulverized coal and waste tire-derived fuel (as well as two polymers, PS and PMMA) were burned in this work. A correlation between CO and PAHs was found with the particle number density (also expressed as the bulk equivalence ratio, ϕ) in the furnace. As the CO emissions increased with increasing bulk ϕ, so did the PAH emissions when the furnace temperature was kept unchanged. As bulk ϕ increased from 0.7 to 2.4, the onset of the increase of CO was at a lower ϕ values than that for the PAHs, which experienced a more delayed but rather exponential response. Thus, CO emissions could be used as

a warning for upcoming PAH emissions in this range of bulk ϕ, which is typical of practical applications. However, an inverse correlation of CO and PAHs was observed with the furnace gas temperature. Raising the gas temperature from 1000 to 1300 °C decreased the PAH yields by orders of magnitude to levels below the detection limit herein of 0.7 μg/(g of fuel). On the other hand, the CO yields increased by up to a factor of 3, which was mostly attributed to the history of the carbon (soot and char) in the furnace and its oxidation characteristics. Thus, at elevated furnace temperatures, high CO partial pressures may give a false warning on the PAH emissions.

Acknowledgments

This research was partially supported by NSF Grant BES-9505703. The authors would like to acknowledge technical help from Prof. Paul Vouros.

Literature Cited

(1) Howard, J. B.; Longwell, J. P.; Marr, J. A.; Pope, C. J.; Busby, W. F.; Lafleur, A. L.; Taghizadeh, K. *Combust. Flame* **1995**, *101*, 262−270.
(2) Longwell, J. F. *Nineteenth Symposium (International) on Combustion*; The Combustion Institute: Pittsburgh, PA, 1982; pp 1339−1350.
(3) Beér, J. M. *Twenty-Second Symposium (International) on Combustion*; The Combustion Institute: Pittsburgh, PA, 1988; pp 1−16.
(4) Seeker, W. R.; Koshland, C. P. *Combust. Sci. Technol.* **1990**, *74*, i−viii.
(5) LaFond, R. K.; Kramlich, J. C.; Seeker, W. R.; Samuelson, G. S. *J. Air Pollut. Control Assoc.* **1985**, *35*, 658.
(6) Lemieux, P. M. EPA-600-R-94-070. Apr 1994.
(7) Staley, J. L.; Richards, M. K.; Huffman, G. L.; Olexey, R. A.; Dellinger, B. *JAPCA* **1989**, *39*, 321−327.
(8) Frenklach, M. *Combust. Sci. Technol.* **1990**, *74*, 283−296.
(9) Levendis, Y. A.; Atal, A.; Carlson, J.; Dunayevskiy, Y.; Vouros, P. *Environ. Sci. Technol.* **1996**, *30* (9), 2742−2754.
(10) Atal, A.; Levendis, Y. A.; Carlson, J.; Vouros, P. *Combust. Flame* **1997**, *110*, 462−478.
(11) Panagiotou, T.; Levendis, Y. A.; Carlson, J.; Vouros, P. *Proceedings of the Twenty-Sixth Symposium (International) on Combustion*; The Combustion Institute: Pittsburgh, PA, 1996; pp 2421−2430.
(12) Leung, D. Y. C.; Lam, G. C. K. 3rd Asian-Pacific International Symposium on Combustion and Energy Utilization, 1995.
(13) Atal, A.; Levendis, Y. A. *Fuel* **1995**, *74* (11), 1570.
(14) Atal, A.; Steciak, J.; Levendis, Y. A. *Fuel* ***1995***, *74* (4), 495.
(15) Wheatley, L.; Levendis, Y. A.; Vouros, P. *Environ. Sci. Technol.* Vol. 27, **1993**, *27*, 2885−2895.
(16) Steciak, J.; Levendis, Y. A.; Wise, D. L. *AIChE J.* **1995**, *41*, 712.
(17) Cumper, J. G.; Levendis, Y. A.; Metghalchi, M. Presented at the Symposium on Heat and Mass Transfer in Fire and Combustion Systems, ASME Winter Annual Meeting, Dallas, TX, ASME Publication HTD-148, Nov 25−30, 1990.
(18) Atal, A.; Levendis, Y. A.; Carlson, J. *Combust. Sci. Technol.* **1998**, *131*, 147.
(19) Jones, P. W. Polynuclear Aromatic Hydrocarbons. In *Handbook of Carcinogens and Hazardous Substances*; Bowman, M. C., Ed.; Marcel Dekker: New York, 1977.
(20) Williams, P. T. *J. Inst. Energy* **1992**, *65*, 46−54.
(21) Courtemanche, B.; Levendis, Y. A. *Fuel* **1998**, *77*, 183−196.
(22) Reynolds, W. C. *STANJAN Equilibrium Program*; Stanford University: Stanford, CA, 1986.
(23) Arthur, J. *Trans. Faraday Soc.* **1951**, *47*, 164−178.
(24) Rossberg, M. Z. *Elektrochem.* **1956**, *60*, 952.
(25) Phillips, R.; Vastola, F. J.; Walker, P. L., Jr. *Carbon* **1970**, *8*, 205.
(26) Young, B. C.; Niksa, S. *Fuel* **1988**, *67*, 155−164.
(27) Tognotti, L.; Longwell, J. P.; Sarofim, A. F. *Twenty-Third Symposium (International) on Combustion*; The Combustion Institute: Pittsburgh, PA, 1990; 1207−1213.
(28) Mitchell, R. E. *Twenty-Second Symposium (International) on Combustion*; The Combustion Institute: Pittsburgh, PA, 1988, 69-78.
(29) Waters, B. J.; Squires, R. G.; Laurendeau, N. M.; Mitchell, R. E. *Combust. Flame* **1988**, *74*, 91−106.
(30) Hurt, R. H.; Mitchell, R. E. *Twenty-Fourth Symposium (International) on Combustion*; The Combustion Institute: Pittsburgh, PA, 1992; 1243−1250.
(31) Zeng, T.; Fu, W. B. *Combust. Flame* **1996**, *107*, 197−210.
(32) Flagan, R. C.; Seinfeld, J. H. *Fundamentals of Air Pollution Engineering*; Prentice Hall: Englewood Cliffs, NJ, 1988.
(33) Fenimore, C. P.; Moore, J. *Combust. Flame* **1974**, *22*, 343−351.

Received for review April 17, 1998. Revised manuscript received August 10, 1998. Accepted August 27, 1998.

ES980399F